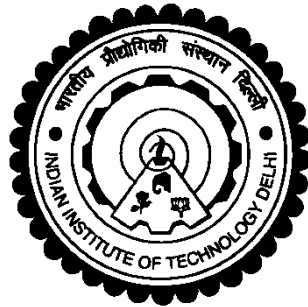


**EXPERIMENTAL INVESTIGATIONS AND CHARACTERIZATION OF
TRACHEAL SCAFFOLDS FABRICATED USING SOLVENT BASED 3D
PRINTING**

RUDRANARAYAN KANDI



DEPARTMENT OF MECHANICAL ENGINEERING

INDIAN INSTITUTE OF TECHNOLOGY DELHI

JUNE 2022

©Indian Institute of Technology Delhi (IITD), 2022

**EXPERIMENTAL INVESTIGATIONS AND CHARACTERIZATION OF
TRACHEAL SCAFFOLDS FABRICATED USING SOLVENT BASED 3D
PRINTING**

by

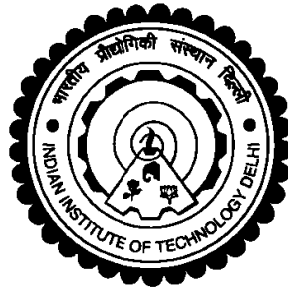
Rudranarayan Kandi

DEPARTMENT OF MECHANICAL ENGINEERING

Submitted

in fulfilment of the requirements of the degree of Doctor of Philosophy

to the



INDIAN INSTITUTE OF TECHNOLOGY DELHI

JUNE 2022

DEDICATED TO

LORD JAGANNATH, MY PARENTS AND LOVED ONES

Certificate

This is to certify that the thesis entitled '**Experimental investigations and characterization of tracheal scaffolds fabricated using solvent based 3D printing**' submitted by **Mr. Rudranarayan Kandi** to the Indian Institute of Technology Delhi, for the award of the degree of *Doctor of Philosophy*, is a record of the original bonafide research work carried out by him under my guidance and supervision. The results contained in it have not been submitted in part or full to any other institute or university for the award of any degree/diploma.



(Dr. Pulak Mohan Pandey)

Professor

Department of Mechanical Engineering

Indian Institute of Technology Delhi

Acknowledgments

This thesis symbolizes an important milestone in the journey of my life. I express my deep sense of gratitude and sincere thanks to my thesis supervisor *Prof. P. M. Pandey*. His excellent guidance, constant encouragement and optimistic outlook have been a source of motivation for me throughout this work. His knowledge of the subject and wealth of experience steered me to complete the work. My interaction with him has been a great learning experience. I am immensely benefited by his devotion for the research, his ability to see things that are not obvious and their perseverance to pursue creative leads in research. Besides being a source of immense knowledge and experience, *Prof. P. M. Pandey* is very kind and caring with great compassion and love for the students. I will forever cherish my close association with him.

I gratefully acknowledge the fellowship provided by the *Ministry of Human Resource and Development (MHRD), India*, for carrying out this work. The author gratefully acknowledges the support provided by the *Multi International Faculty Interdisciplinary Research Project (MFIRP, Grant no- MI02065)* between IIT Delhi and AIIMS Delhi for carrying our experimental works.

I express my deep sense of gratitude to *Prof. P. Venkateswara Rao, Prof. Sudarsan Ghosh, Prof. Bhabani. K. Satapathy* for being part of my student research committee and thankful for their constructive criticism and valuable guidance during the course of presentations. I am thankful to lab staff members *Mr Viveka Bikasha Satpathy., Mr. Vikas Khatkar, and Mr. Subash Chand* for providing me essential aids to complete experimentation work for the thesis.

I am also thankful to the office staff member *Mr. Kishan Kumar* for his support in the day to day activities. I am thankful to my seniors, and research scholars at IITD *Dr. Girish Chandra Verma, Dr. Pawan Sharma, Dr. Dayanidhi K. Pathak, Dr. Gurminder Singh, Dr.*

Ravinder pal Singh, Dr. Jasvinder Singh, Dr. Ajit Kumar, Dr. Usha Rani Rath, Dr. Dipesh Mishra, Dr. Mayank Srivastava, Dr. Avinash Raulo, Dr. Prateek Khatri, Mr. Saroj K Samantaray, Mr. Ashok Bakshi, Mr. Sailendu Biswal, Mr. Gaurav Tripathy, Mr. Shitanshu Arya, Mr. Arun Kumar, Mr. Priyabrata Das, Mrs. Garima Dixit and co-research scholars/ friends at IIT Delhi who were always there to lend a helping hand when it mattered the most and for the camaraderie that took away all the pressures and made research work more enjoyable. I am deeply grateful to Mr. Tushar Mishra and friends for providing stimulating discussions and happy distractions to rest my mind outside my research work.

I am grateful to *Prof. Sujata Mohanty, Mrs. Misba Majood, Mr. Kunj Sachdeva, and Dr. Manu Dalela* of DBT- Stem Cell Facility, Centre of Excellence for Stem cell Research, All India Institute of Medical Sciences, New Delhi for their help in biological assessments.

I am indebted to my parents, *Shri Kshirod Kumar Kandi, Smt. Kanaklata Das and Smt. Nalini Prava Das* for their blessings, motivation and constant support throughout this period. I am thankful to everyone who helped me directly or indirectly to complete this work. I am also grateful to *Lord Jagannath, the Almighty*, for having blessed me to rise and take up this challenge.

(Rudranarayan Kandi)

Abstract

Tracheal reconstruction remains a major therapeutic challenge due to the unavailability of donors and the lack of biomimetic tubular grafts. Anastomosis, an end to end surgery, is a solution to circumferential damage, tumour and stenosis in the trachea. However, it is limited when a lesion is extended to one-third of the tracheal length and half of the length for child and adult individuals respectively. Allograft could be an alternative to the damaged trachea. However, lifelong immunotherapy and the unavailability of the donor have limited the transplant process. Hence, tissue-engineered synthetic implants of matched rigidity and flexibility with appropriate regeneration offer a promising solution to repair long-segment tracheal stenosis. Artificial tubular scaffolds fail to imitate the natural rigidity and flexibility of the organ. Therefore, a trade-off between strength and flexibility asks for customized scaffolds with enhanced flexibility and adequate rigidity. Limited work has been reported that discusses the customization of shape and manipulation of material for tracheal scaffolds to match with the biomechanical properties of the native trachea.

In order to fill this research gap, customized tubular scaffolds for tracheal tissue engineering with a novel route using solvent-based extrusion 3D printing were successfully fabricated. The manufacturing approach involved the extrusion of polymeric ink over a rotating predefined pattern to construct the customized tubular structure of polycaprolactone (PCL) and polyurethane (PU). The rheological properties were investigated to study the flow behaviour and characterization of the solutions used for 3D printing. Dimensional deviations in thickness of the fabricated scaffolds were calculated for various layer thicknesses of 3D printing. Morphological and Physiochemical properties of scaffolds were investigated by Scanning electron microscope (SEM), contact angle measurement, and Fourier Transform Infrared Spectroscopy (FTIR). Preliminary mechanical assessments illustrated comparable mechanical

properties with the native human trachea. Furthermore, the scaffolds were found to be biocompatible to promote cell adhesion from the preliminary *in vitro* cytotoxicity results.

No work has been done to study the effects of 3D printing parameters on the print quality and the mechanical properties of tubular scaffolds. The work aims to fill the gaps by investigating the effects of 3D printing parameters like infill density, layer thickness and print speed on print quality and mechanical characteristics. Experimental runs were planned as per the central composite design (CCD) to evaluate the effects of input parameters on the output responses. The printing quality was quantified by measuring the average surface roughness of the printed scaffolds and mechanical properties were evaluated by measuring radial compressive load, and percentage elongation. The experimental investigations revealed that printing quality was improved at higher infill densities and was deteriorated at higher print speeds and layer thicknesses. Similarly, the radial compressive load was improved with the increase in infill density and was decreased with an increase in layer thickness, print speed, and percentage of PU. The percentage elongation was found to improve at higher infill densities and percentages of PU and was reduced with an increase in layer thickness and print speed. Additionally, a multi-objective optimization using Genetic Algorithm was used to evaluate the optimum conditions to minimize surface roughness and maximize radial compression load and percentage elongation. Finally, a case study was performed from the existing reports and the results of the present work.

It could be elucidated from the literature that there exists a scope to investigate in the field of customization of tubular scaffolds to manipulate the biomechanical properties without compromising the graft rejection. Hence, customized tubular scaffolds of polycaprolactone (*PCL*) and polyurethane (*PU*) similar to the goat trachea were fabricated using solvent-based extrusion 3D printing. Three different types of scaffolds namely cylindrical, bellow shaped and spiral scaffolds equivalent to the dimension of native goat trachea were fabricated. Mechanical

investigations were performed for all combinations of formulations with various scaffold shapes. The results were compared with native tracheal properties to find out suitable formulations with matched mechanical properties. Spiral shaped scaffolds were found to be the desired shape maintaining clear patency when subjected to longitudinal compression and torsion load equivalent to the neck flexion and rotation.

Furthermore, the synthetic tracheal scaffolds were coated with natural polymers, mixture of alginate and gelatin using solvent-based 3D printing to improve the biocompatibility of the overall tracheal scaffolds. Optimum combinations of inks were found by evaluating the dimensional stability for each formulation during 3D printing. Rheological characteristics were investigated to study the flow behaviour of the formulated inks. The coated scaffolds were characterized by various physical, morphological, and mechanical characterizations. The coated tracheal scaffolds yielded hydrophilic surfaces by reducing contact angle by approximately 70% compared to the uncoated synthetic tracheal scaffolds. Radial compression test results showed coated scaffolds offered excellent radial strength compared to the strength of native rat trachea.

In vitro degradation test was performed by immersing the scaffolds in phosphate buffer solution (PBS) for 16 weeks to check for long term implantation. The printed uncoated scaffolds were further evaluated for biological assay using bone marrow-derived human mesenchymal stem cells (hMSCs). All the scaffolds were proved to promote cell proliferation and adhesion, though PCL70/PU30 combinations yielded the highest biocompatibility among the uncoated scaffolds. Additionally, the biological assay for coated scaffolds showed excellent compared to the uncoated scaffolds. Among all the coated scaffolds, PCL70/PU30 coated with alginate 2%/ gelatin 4% (A2G4) was found to be the best biocompatible candidate for the tracheal regenerative application.

सार

दाताओं की अनुपलब्धता और बायोमिमेटिक ट्यूबलर ग्राफ्ट की कमी के कारण श्वासनली का पुनर्निर्माण एक प्रमुख चिकित्सीय चुनौती बनी हुई है। एनास्टोमोसिस, एंड टू एंड सर्जरी, श्वासनली में परिधीय क्षति, ट्यूमर और स्टेनोसिस का समाधान है। हालाँकि, यह तब सीमित होता है जब एक घाव श्वासनली की लंबाई के एक तिहाई और बच्चे और वयस्क व्यक्तियों के लिए क्रमशः आधी लंबाई तक फैल जाता है। एलोग्राफ्ट क्षतिग्रस्त श्वासनली का एक विकल्प हो सकता है। हालांकि, आजीवन इम्यूनोथेरेपी और दाता की अनुपलब्धता ने प्रत्यारोपण प्रक्रिया को सीमित कर दिया है। इसलिए, उपयुक्त पुनर्जनन के साथ मिलान कठोरता और लचीलेपन के ऊतक-इंजीनियर सिंथेटिक प्रत्यारोपण लंबे खंड वाले ट्रेकिअल स्टेनोसिस की मरम्मत के लिए एक आशाजनक समाधान प्रदान करते हैं। कृत्रिम ट्यूबलर मचान अंग की प्राकृतिक कठोरता और लचीलेपन की नकल करने में विफल होते हैं। इसलिए, ताकत और लचीलेपन के बीच एक तालमेल अनुकूलित लचीलेपन और पर्याप्त कठोरता के साथ अनुकूलित मचानों की मांग करता है। सीमित कार्य की सूचना मिलती है जो देशी श्वासनली के जैव-यांत्रिक गुणों के साथ मेल खाने के लिए श्वासनली मचानों के लिए आकार के अनुकूलन और सामग्री के हेरफेर पर चर्चा करती है।

इस शोध अंतर को भरने के लिए, सॉल्वेंट-आधारित एक्सट्रूजन 3 डी प्रिंटिंग का उपयोग करके एक नवीन मार्ग के साथ श्वासनली ऊतक इंजीनियरिंग के लिए अनुकूलित ट्यूबलर मचान सफलतापूर्वक बनाये

गए थे। विनिर्माण दृष्टिकोण में पॉलीकैप्रोलैक्टोन (पीसीएल) और पॉलीयूरेथेन (पीयू) की अनुकूलित ट्यूबलर संरचना का निर्माण करने के लिए एक घूर्णन पूर्वनिर्धारित पैटर्न पर बहुलक स्याही को बाहर निकालना शामिल था। 3 डी प्रिंटिंग के लिए उपयोग किए जाने वाले समाधानों के प्रवाह व्यवहार और लक्षण वर्णन का अध्ययन करने के लिए रियोलॉजिकल गुणों की जांच की गई। बनाये हुए मचानों की मोटाई में आयामी विचलन की गणना 3 डी प्रिंटिंग की विभिन्न परत मोटाई के लिए की गई थी। स्कैनिंग इलेक्ट्रॉन माइक्रोस्कोप (एसईएम), संपर्क कोण माप, और फूरियर ट्रांसफॉर्म इन्फ्रारेड स्पेक्ट्रोस्कोपी (एफटीआईआर) द्वारा स्कैफोल्ड के रूपात्मक और भौतिक रासायनिक गुणों की जांच की गई। प्रारंभिक यांत्रिक आकलन ने मूल मानव श्वासनली के साथ तुलनीय यांत्रिक गुणों को चित्रित किया। इसके अलावा, इन विट्रो साइटोटोक्सिसिटी परिणामों में प्रारंभिक से सेल आसंजन को बढ़ावा देने के लिए मचानों को जैव-संगत पाया गया।

प्रिंट गुणवत्ता और ट्यूबलर मचानों के यांत्रिक गुणों पर 3डी प्रिंटिंग मापदंडों के प्रभावों का अध्ययन करने के लिए कोई काम नहीं किया गया है। कार्य का उद्देश्य प्रिंट गुणवत्ता और यांत्रिक विशेषताओं पर इनफिल घनत्व, परत की मोटाई और प्रिंट गति जैसे 3 डी प्रिंटिंग मापदंडों के प्रभावों की जांच करके अंतराल को भरना है। आउटपुट प्रतिक्रियाओं पर इनपुट मापदंडों के प्रभावों का मूल्यांकन करने के लिए केंद्रीय समग्र डिजाइन (सीसीडी) के अनुसार प्रायोगिक रन की योजना बनाई गई थी। मुद्रित मचानों की औसत सतह खुरदरापन को मापकर

मुद्रण गुणवत्ता की मात्रा निर्धारित की गई थी और यांत्रिक गुणों का मूल्यांकन रेडियल कंप्रेसिव लोड और बढ़ाव के प्रतिशत को मापकर किया गया था। प्रयोगात्मक जांच से पता चला है कि मुद्रण गुणवत्ता उच्च इनफिल घनत्व से सुधरी तथा उच्च प्रिंट गति और परत मोटाई से खराब हुई। इसी तरह, रेडियल कंप्रेसिव लोड में इन्फिल घनत्व में वृद्धि के साथ सुधार हुआ था और परत की मोटाई, प्रिंट गति और पीयू के प्रतिशत में वृद्धि के साथ घट गया था। बढ़ाव का प्रतिशत पीयू के उच्च इन्फिल घनत्व और प्रतिशत में सुधार पाया गया था और परत मोटाई और प्रिंट गति में वृद्धि के साथ कम हो गया था। इसके अतिरिक्त, जेनेटिक एल्गोरिथम का उपयोग करते हुए एक बहु-उद्देश्य अनुकूलन का उपयोग सतह खुरदरापन को कम करने और रेडियल संपीड़न भार और बढ़ाव के प्रतिशत को अधिकतम करने के लिए इष्टतम स्थितियों का मूल्यांकन करने के लिए किया गया था। अंत में, मौजूदा रिपोर्टों और वर्तमान कार्य के परिणामों से एक केस स्टडी की गई।

साहित्य से यह स्पष्ट किया जा सकता है कि ग्राफ्ट अस्वीकृति से समझौता किए बिना बायोमेकेनिकल गुणों में हेरफेर करने के लिए ट्यूबलर मचानों के अनुकूलन के क्षेत्र में जांच करने की गुंजाइश मौजूद है। इसलिए, बकरी ट्रेकिआ के समान पॉलीकैप्रोलैक्टोन (पीसीएल) और पॉलीयुरेथेन (पीयू) के अनुकूलित ट्यूबलर मचान विलायक-आधारित एक्सट्रूज़न 3 डी प्रिंटिंग का उपयोग करके बनाये गए थे। देशी बकरी श्वासनली के आयाम के बराबर तीन अलग-अलग प्रकार के मचान अर्थात् बेलनाकार, बोले आकार और सर्पिल मचान बनाये गए थे। विभेदक स्कैनिंग कैलोरीमेट्री परिणामों

ने पीसीएल मैट्रिक्स में पीयू को शामिल करके मचानों में इलास्टोमेरिक प्रकृति में सुधार की पुष्टि की। विभिन्न मचान आकृतियों के साथ योगों के सभी संयोजनों के लिए यांत्रिक जांच की गई। मिलान किए गए यांत्रिक गुणों के साथ उपयुक्त योगों का पता लगाने के लिए परिणामों की तुलना देशी श्वासनली के गुणों से की गई। अनुदैर्घ्य संपीड़न और गर्दन के लचीलेपन और रोटेशन के बराबर मरोड़ भार के अधीन होने पर सर्पिल आकार के मचानों को स्पष्ट धैर्य बनाए रखने के लिए वांछित आकार के रूप में पाया गया। इसके अलावा, समग्र श्वासनली मचानों की जैव-रासायनिकता में सुधार करने के लिए विलायक-आधारित 3 डी प्रिंटिंग का उपयोग करके सिंथेटिक ट्रेकिअल मचानों को प्राकृतिक पॉलिमर, ऐल्लिजनेट और जिलेटिन का मिश्रण के साथ लेपित किया गया था। 3 डी प्रिंटिंग के दौरान प्रत्येक फॉर्मूलेशन के लिए आयामी स्थिरता का मूल्यांकन करके स्याही के इष्टतम संयोजन पाए गए। तैयार स्याही के प्रवाह व्यवहार का अध्ययन करने के लिए रियोलॉजिकल विशेषताओं की जांच की गई। लेपित मचानों में विभिन्न भौतिक, रूपात्मक और यांत्रिक लक्षणों की विशेषता की गई। एक्स-रे विवर्तन (एक्सआरडी) ने कोटिंग का प्रदर्शन करके समग्र मचानों की अनाकार प्रकृति में वृद्धि का संकेत दिया। एफटीआईआर परिणामों ने संकेत दिया कि प्राकृतिक पॉलिमर को मोड़ते समय कोई रासायनिक प्रतिक्रिया नहीं हुई थी। लेपित श्वासनली मचानों ने अलेपित सिंथेटिक श्वासनली मचानों की तुलना में संपर्क कोण को लगभग 70% तक कम करके हाइड्रोफिलिक सतह प्राप्त की। रेडियल

संपीडन परीक्षण के परिणामों से पता चला है कि लेपित मचानों ने देशी चूहे की श्वासनली की ताकत की तुलना में उत्कृष्ट रेडियल ताकत की पेशकश की है।

लंबी अवधि के आरोग्य की जांच के लिए 16 सप्ताह के लिए फॉस्फेट बफर घोल (पीबीएस) में मचानों को डुबो कर इन विट्रो गिरावट परीक्षण किया गया था। अस्थि मज्जा-व्युत्पन्न मानव मेसेनकाइमल स्टेम सेल (hMSCs) का उपयोग करके जैविक परख के लिए मुद्रित अलेपित मचानों का मूल्यांकन किया गया था। सभी मचानों को सेल प्रसार और आसंजन को बढ़ावा देने के लिए साबित किया गया था, हालांकि PCL70 / PU30 संयोजनों ने अलेपित मचानों के बीच उच्चतम जैव-रासायनिकता प्राप्त की। इसके अतिरिक्त, लेपित मचानों के लिए जैविक परख ने अलेपित मचानों की तुलना में उत्कृष्ट दिखाया। सभी लेपित मचानों के बीच, ऐल्लिजनेट 2% / जिलेटिन 4% (A2G4) के साथ लेपित PCL70 / PU30 श्वासनली पुनर्योजी अनुप्रयोग के लिए सबसे अच्छा जैव-संगत उम्मीदवार पाया गया।

Contents

Certificate.....	i
Acknowledgments.....	ii
Abstract.....	iv
सार.....	vii
Contents	xii
List of Figures.....	xviii
List of Tables	xxiv
Acronym	xxvi
Nomenclature.....	xxviii
Chapter 1 Introduction.....	1
1.1 Introduction	2
1.1.1 Trachea.....	2
1.1.2 Diseases associated with trachea	3
1.1.3 Problems associated with airway stents.....	3
1.1.4 Utility of tissue-engineered tracheal scaffolds.....	4
1.1.5 Fabrication of customized tracheal scaffolds.....	5
1.1.6 Three dimensional (3D) printing	7
1.1.7 Motivation for the current study	8

1.1.8	Thesis organization	9
Chapter 2	Literature review and research objectives.....	11
2.1	Literature review	12
2.1.1	Tracheal implantations.....	12
2.1.2	Materials for tracheal scaffolds.....	14
2.1.3	Fabrication methods.....	16
2.2	Research gaps	21
2.3	Goal of the present research work.....	22
2.3.1	Research Objectives.....	22
Chapter 3	Fabrication of tracheal scaffolds using solvent-based extrusion 3D printing....	23
3.1	Introduction	24
3.2	Materials and method.....	25
3.2.1	Materials	25
3.2.2	Rheological study.....	25
3.2.3	Scaffold fabrication procedure.....	26
3.3	Characterization	29
3.3.1	Morphology of scaffold	29
3.3.2	Fourier transform infrared spectroscopy (FTIR)	29
3.3.3	Contact angle measurement	29
3.3.4	Mechanical characterization	30

3.3.5	Biological assessment	31
3.4	Results and discussion.....	32
3.4.1	Rheological characteristics of ink.....	32
3.4.2	Scaffold morphology	35
3.4.3	Fourier transformation infrared spectroscopy.....	36
3.4.4	Contact angle	37
3.4.5	Mechanical characterization	38
3.4.6	Biological test result	40
3.5	Conclusions	42
Chapter 4	Experimental investigations on print quality, mechanical properties, and process optimization	44
4.1	Introduction	45
4.2	Selection of process parameters for the fabrication method	46
4.2.1	Plan of Experimentation	46
4.3	Experimental investigations	48
4.3.1	Surface roughness measurement.....	48
4.3.2	Radial compressive load measurement.....	48
4.3.3	Elongation measurement.....	49
4.4	Statistical modelling of responses	50
4.5	Results and discussion.....	53

4.5.1	Effect of process parameters on surface roughness	54
4.5.2	Effect of process parameters on radial compressive load	61
4.5.3	Effect of process parameters on the percentage elongation.....	65
4.5.4	Multi-objective optimization	69
4.5.5	Case study	72
4.6	Conclusions	74
Chapter 5 Morphological, physicochemical, and biomechanical characterizations of developed customized tracheal scaffold		
		76
5.1	Materials and method	77
5.1.1	Scaffold fabrication.....	77
5.1.2	Scaffold morphology	77
5.1.3	Thermal characterization	78
5.1.4	Mechanical characterization	79
5.2	Results	79
5.2.1	Morphological characterization	79
5.2.2	Thermal characterization	81
5.2.3	Mechanical characterization	83
5.3	Discussion	87
5.4	Conclusions	90

Chapter 6	Fabrication and characterization of natural polymer coating over 3D printed synthetic graft.....	92
6.1	Introduction.....	93
6.2	Materials and method.....	93
6.2.1	Materials.....	94
6.2.2	Solution preparation and coating over the 3D printed scaffolds.....	94
6.3	Characterization.....	94
6.3.1	Assessment of printability.....	94
6.3.2	Rheological characterization.....	95
6.3.3	Morphology of coated tubular scaffolds.....	96
6.3.4	X-Ray Diffraction (XRD).....	97
6.3.5	Fourier transmittance infrared spectroscopy (FTIR).....	97
6.3.6	Contact angle measurement.....	97
6.3.7	Mechanical characterization.....	97
6.4	Results and discussion.....	98
6.4.1	Printability of the inks.....	98
6.4.2	Rheological characterization.....	100
6.4.3	Morphology of coated scaffolds.....	103
6.4.4	X-Ray Diffraction (XRD).....	104
6.4.5	Fourier transmittance infrared spectroscopy (FTIR).....	105

6.4.6	Contact angle measurement	106
6.4.7	Mechanical characterization	107
6.5	Conclusions	108
Chapter 7	<i>In vitro</i> characterization and cytocompatibility assessment of 3D printed tracheal scaffolds	110
7.1	Introduction	111
7.2	Materials and method	111
7.2.1	<i>In vitro</i> degradation	111
7.2.2	<i>In vitro</i> biological assessment	112
7.3	Results and discussion	114
7.3.1	<i>In vitro</i> degradation	114
7.3.2	<i>In vitro</i> biological assessment of uncoated scaffolds	117
7.3.3	<i>In vitro</i> biological assessment of coated scaffolds	121
7.4	Conclusions	123
Chapter 8	Major conclusions and Future scope	125
8.1	Conclusions	126
8.2	Future scope	128
References	129
List of Publications	148
Biodata	150

List of Figures

Figure 2-1 (a) Moulding method for the fabrication of tubular scaffolds, (b) the mould for preparation of the PCL tracheal tube, (c) gross appearance of PCL tube with SEM micrographs of outer and inner surfaces and (d) gross appearance of PCL tube with inner surface coated with gelatin. Reproduced/adapted from the ref. ²⁵	17
Figure 2-2 (a) Schematic diagram of general single-nozzle electrospinning for BLTS, (b) optical image of BLTS, and (c) SEM images of the cross-section of the BLTS. Reproduced/adapted from ref. ⁷⁷	18
Figure 2-3 (a) Illustration of developed 3D printing method; (b) fabrication of different types of customized tracheal scaffolds. Reproduced/adapted from the ref. ⁶⁶	20
Figure 3-1 Flow chart of the methodology for the fabrication of customized tubular scaffolds	27
Figure 3-2 (a) Illustration of developed methodology, (b) Fabrication of different types of customized tracheal scaffolds and representative SEM image illustrating the thickness and wall architecture of 3D printed tracheal wall, and (c) Measurements of thickness of scaffold using optical microscopy	28
Figure 3-3 Illustration of mechanical characterizations (a) Tensile test and (b) Radial compression test of tracheal scaffolds.	31
Figure 3-4 (a) Viscosity as a function of shear rate for PCL, PCL/PU and PU blends, (b) Loss modulus (G''), (c) Storage modulus (G') as a function of angular frequency (ω) for all the solutions, and (d) Viscosity as a function of time to investigate the viscosity recovery percentage of all the solutions during 3iTT test.....	34

Figure 3-5 FTIR spectra in terms of transmittance of 3D printed PCL, PCL/PU, and PU blends.
.....37

Figure 3-6 Contact angle measurements of (a) as fabricated, and (b) plasma treated PCL, PCL/PU and PU scaffolds.....38

Figure 3-7 (a) Tensile testing of polymeric PCL, PCL/PU and PU samples, and (b) Elastic moduli in comparison with native human trachea. The data represents mean \pm SD of three independent experiments.39

Figure 3-8 (a) Radial compression of 3D printed polymeric human tracheal scaffolds, and (b) Load carrying capacity at 50% reduction of scaffold diameter during radial compression. The data represents mean \pm SD of three independent experiments.40

Figure 3-9 SEM images of scaffold surfaces (a) without cell seeding, and (b-e) with cell seeding surfaces (Magnification: 3000 X and Scalebar: 20 μ m).41

Figure 3-10 Hemolytic activity in Red Blood Cells (RBCs) of 3D printed PCL, PCL/PU and PU scaffolds. The data represents mean \pm SD of three independent experiments.41

Figure 4-1 Illustration of scaffolds at various layer thicknesses of (a) 0.05 mm (Inaccurate printing), (b) 0.1 mm, (c) 0.14 mm, (d) 0.18 mm, (e) 0.22 mm, and (f) 0.26 mm. The images were taken at magnification: 20X.47

Figure 4-2 Illustration of experimental methods measuring (a) surface roughness, (b) radial compressive load, and (c) circumferential elongation50

Figure 4-3 (a) Fabricated tubular graft, (b) cross-sectional view of the graft, (c) SEM image of the cross-sectional view of a cut section from the graft (Magnification: 60X), and (d) XRD plot for PCL, PCL/PU and PU solution55

Figure 4-4 SEM images of the walls of fabricated grafts at fixed infill density of 50 %, print speed of 5 mm/S, percentage of PU (50%) and at different layer thicknesses of (a) 0.1 mm, (b) 0.14 mm, (c) 0.18 mm, (d) 0.22 mm, and (e) 0.26 mm. The images were taken at magnification: 100X.....56

Figure 4-5 (a) Main effects plot and (b) Percentage of contributions of factors and interactions for average surface roughness (Ra).....57

Figure 4-6 SEM images of scaffold surfaces at various infill densities of (a) 30%, (b) 40%, (c) 50%, (d) 60%, and (e) 70%. The images were taken at magnification: 500X.....58

Figure 4-7 The surface quality of fabricated scaffolds at (a) 3 mm/S and (b) 7 mm/S. The images were taken at magnification: 500X.....59

Figure 4-8 (a) Surface plot, and (b) interaction plot for Infill density and Layer thickness60

Figure 4-9 (a) Surface plot and (b) interaction plot for layer Thickness and Print Speed.....61

Figure 4-10 3D topography of scaffold surfaces printed at (a) Layer thickness of 0.26 mm and print speed of 3 mm/s, and (b) Layer thickness of 0.26 mm and print speed of 7 mm/s.....61

Figure 4-11 Main effects plot and (b) Percentage of contributions of factors and interactions for the radial compressive load (N)64

Figure 4-12 Illustration of voids or gaps among rasters at layer thicknesses of (a) 0.1 mm and (b) 0.26 mm.....65

Figure 4-13 (a) Surface plot, and (b) interaction plot for Layer Thickness and percentage of PU65

Figure 4-14 (a) Main effects plot and (b) Percentage of contributions of factors and interactions for Elongation (%)67

Figure 4-15 (a) Surface plot, and (b) interaction plot for Print speed and percentage of PU ..	69
Figure 4-16 Pareto solution for a given set of responses	71
Figure 4-17 Illustration of 3D printing of customized axisymmetric scaffolds of various shapes and sizes	74
Figure 5-1 Portion of native goat trachea. Various tracheal scaffolds (b) cylindrical, (c) spiral, and (d) bellow shaped equivalent to the dimension of native goat trachea.	80
Figure 5-2 (a) Representative SEM images illustrating scaffold surfaces (Magnification: 500 X) and (b) AFM micrographs for PCL, PCL/PU and PU samples.....	81
Figure 5-3 (a) TGA thermographs for PCL, PCL/PU and PU. DSC thermographs of samples during (b) heating cycle and (c) cooling cycle.....	82
Figure 5-4 Peak load during radial compression test for (a) cylindrical scaffolds (b) bellow shaped scaffolds, and (c) spiral-shaped scaffolds. Load vs displacement curve during cyclic compression in 1 st cycle and 300 th cycle for (d, g) cylindrical scaffolds (e, h) bellow shaped scaffolds, and (f, i) spiral-shaped scaffolds for PCL, PCL/PU and PU and goat native trachea. The data represents mean \pm SD of three independent experiments.	85
Figure 5-5 (a) Load vs displacement obtained from longitudinal compression. Illustration of various scaffolds (b) cylindrical, (c) spiral, and (d) bellow shaped subjected to longitudinal compression. (e) Torque generated by rotating the scaffolds during torsion. Illustration of various scaffolds (f) cylindrical, (g) spiral, and (h) bellow shaped subjected to torsion.	86
Figure 6-1 Printability evaluation of (a, b) less viscous (under gelation), (c, d) optimum viscous (proper gelation), (e, f) more viscous (over gelation) ink during the extrusion printing, (g) Dimensional deviations of all the formulated inks. The data represents mean \pm SD of three independent experiments.	100

Figure 6-2 Apparent viscosity as a function strain rate for A2G4, A3G3 and A4 solutions. 102

Figure 6-3 Storage and loss modulus as a function of angular frequency for A2G4, A3G3 and A4 solutions. 102

Figure 6-4 Apparent viscosity as a function time in shear recovery test (3iTT) for A2G4, A3G3, and A4 solutions. 103

Figure 6-5 (a) Illustration of macroscopic images of the coated scaffold, and (b) SEM images of the cross-sectional view of the coated tracheal scaffold. Surface morphology of (c) uncoated scaffold and (d) coating of the scaffold. 104

Figure 6-6 X-Ray diffraction of PCL/PU, alginate, gelatin and PCL/PU coated with alginate. 105

Figure 6-7 FTIR spectrum for scaffolds coated with alginate, alginate/gelatin. 106

Figure 6-8 (a) Illustration of water droplet absorption over the scaffolds surfaces and (b) contact angle measurements for PCL70/PU30, scaffolds coated with A2G4, A3G3 and A4. The data represents mean \pm SD of three independent experiments. 107

Figure 6-9 Radial compression test of tracheal scaffolds and native trachea (a) Illustration of the test compressing the scaffold and (b) comparison of radial compressive loads for uncoated and various coated scaffolds with native rat trachea. The data represents mean \pm SD of three independent experiments 108

Figure 7-1 (a) weight loss percentages, and (b) Variation in pH of PBS with degraded samples during degradation study for 16 weeks. FTIR spectra of PCL, PCL/PU and PU sample (c) before and (d) after the degradation study 116

Figure 7-2 SEM images illustrating sample surfaces before and after the degradation study 117

Figure 7-3 Cell proliferation over scaffolds assessed by CCK-8 assay (absorbance: 450 nm). TCP was taken as control. (b) Optical fluorescent microscope images of cell staining on the 3D printed PCL, PCL/PU and PU scaffolds. In the images, Green represents: Live Cells and Red represents: Dead Cells. The images were captured at 20X. Cell adhesion and morphology. The data represents mean \pm SD of three independent experiments 119

Figure 7-4 SEM images showing the morphology of hMSCs over various scaffolds after 7 days of incubation, and (b) cell morphologies over PCL70/PU30 at day 7, and 14 120

Figure 7-5 (a) Cell proliferation over uncoated PCL70/PU30 and coated scaffolds assessed by CCK-8 assay (absorbance: 450 nm). TCP was taken as control. (b) Optical fluorescent microscope images of cell staining on the coated 3D printed scaffolds. In the images, Green represents: Live Cells and Red represents: Dead Cells. The images were captured at 20X. The data represents mean \pm SD of three independent experiments 122

Figure 7-6 SEM images showing the morphology of hMSCs over various uncoated PCL70/PU30 scaffold and coated scaffolds after 7 days of incubation..... 123

List of Tables

Table 1-1 List of native tracheae with the dimensions	2
Table 3-1 Estimated rheological coefficients by fitting the curves to the Power law	33
Table 3-2 Viscosity recovery percentages for all the prepared solutions	35
Table 3-3 Variations in measured thicknesses of fabricated tubular scaffolds.....	36
Table 4-1 Process Parameters and their levels used for the experiment.....	47
Table 4-2 Experimental runs.....	52
Table 4-3 Confirmation experiments	53
Table 4-4 Calculated results for FWHM and crystallite size from fitting results.....	54
Table 4-5 Analysis of Variance for average surface roughness after eliminating insignificant terms.....	59
Table 4-6 Analysis of Variance for compressive load after eliminating insignificant terms ..	63
Table 4-7 Analysis of variance for percentage elongation after eliminating insignificant terms	66
Table 4-8 Confirmatory experimentations at the optimum set of parameters	72
Table 4-9 Comparative study with the prior research works.....	73
Table 5-1 Measurement of native goat trachea.....	80
Table 5-2 Thermal results obtained from DSC flow curves for PCL, PCL/PU and PU samples	83
Table 6-1 List of formulations used for 3D printing with their printability	99

Table 6-2 Estimated rheological coefficients by fitting the curves to the Power law 101

Table 6-3 Viscosity recovery percentages for solutions from 3iTT test..... 103

Acronym

3D	Three dimensional
AFM	Atomic Force Microscope
ANOVA	Analysis of Variance
ATR	Attenuated Total Reflection
CAD	Computer Aided Design
CCD	Central Composite Design
CCK	Cell Counting Kit
CSR	Controlled Shear rate
DF	Degree of Freedom
DMEMLG	Low Glucose Dulbecco's Modified Eagle Medium
DMF	Dimethylformamide
DSA	Drop Shape Analyzer
DSC	Differential Scanning Calorimetry
ECM	Extra Cellular Matrix
EDTA	Ethylene diamine tetra acetic acid
ETO	Ethylene dioxide
FBS	Fetal Bovine Serum
FDM	Fused Deposition Modeling
FTIR	Fourier Transform Infrared Spectroscopy
FWHM	Full Width Half Maximum
GA	Genetic Algorithm
hMSCs	Human derived Mesenchymal Stem cells
IPA	Isopropyl Alcohol

LVR	Linear Viscoelastic Region
MS	Mean of Squares
PBS	Phosphate Buffer Solution
PCL	Polycaprolactone
PDS	Polydioxanone
PEG	Polyethylene Glycol
PGA	Polyglycolic Acid
PLGA	Poly(Lactic-Co-Glycolic Acid)
PLLA	Poly(L -Lactide)
PU	Polyurethane
RBC	Red Blood Cell
SEM	Scanning Electron Microscopy
SLA	Stereolithography
SLS	Selective Laser Sintering
SS	Sum of Squares
TCP	Tissue Culture Plate
TET	Tissue Engineered Trachea
THF	Tetrahydrofuran
TGA	Thermogravimetric Analyzer
UTM	Universal Testing Machine
UV	Ultraviolet
XRD	X- Ray Diffraction

Nomenclature

$\dot{\gamma}$	Shear rate
η	Apparent viscosity
β_0	Interception coefficient
β_i	Coefficients for linear terms
β_{ij}	Coefficients for interaction terms
α	Level of significance
Δl	Change in length
λ	Wavelength of radiation
β	FWHM of the peak
2θ	Bragg's angle
τ	Crystallite size
$\% \delta$	Percentage elongation
σ	Tensile strength
ΔH_m	Enthalpy of melting of sample
ΔH_c	Enthalpy of crystallization of sample
ΔH_{100}	Enthalpy of melting of 100% crystalline material
Δd	Dimensional deviation
C=O	Carbonyl group
C-O-C	Ether bond
CH ₂	Methylene group
d_0	Original dimension
d_m	Measured dimension
e	Error

E	Young's modulus
F_c	Compressive load
F_{value}	Fisher's value
$f_1, f_2, \text{ and } f_3$	Objective functions for outputs
G'	Storage modulus
G''	Loss modulus
I_c	Area under crystalline peak/region
I_a	Area under amorphous region
K	Consistency index
k	Dimensionless shape factor
l_0	Original/gauge length
M_n	Molecular weight number
M1	Motor for movement in X axis
M2	Motor for movement in Y axis
M3	Motor for movement in Z axis
n	Flow behavior index
NH ₂	Amino group
OD	Optical density
OH	Hydroxyl group
p	Significance value
R_a	Average surface roughness
R^2	Coefficient of determination
T_g	Glass transition temperature
T_m	Melting temperature

V_e	variance of the error in regression model
W_{PCL}	Fraction of PCL present in the blend
W_0	Weight of dry sample
W_1	Weight of dry degraded sample
χ_c	Relative crystallinity
\hat{y}	Predicted value from the regression model
\hat{y}_{Range}	Range of outputs